AIP | Applied Physics Letters

# Development of stress-induced curved actuators for a tunable THz filter based on double split-ring resonators

Yu-Sheng Lin, You Qian, Fusheng Ma, Zhen Liu, Piotr Kropelnicki et al.

Citation: Appl. Phys. Lett. **102**, 111908 (2013); doi: 10.1063/1.4798244
View online: http://dx.doi.org/10.1063/1.4798244
View Table of Contents: http://apl.aip.org/resource/1/APPLAB/v102/i11
Published by the American Institute of Physics.

# Development of stress-induced curved actuators for a tunable THz filter based on double split-ring resonators

Yu-Sheng Lin,[1] You Qian,[1] Fusheng Ma,[1] Zhen Liu,[1] Piotr Kropelnicki,[2] and Chengkuo Lee[1,a)]

[1]*Department of Electrical and Computer Engineering, National University of Singapore, 4 Engineering Drive 3, Singapore 117576, Singapore*

[2]*Institute of Microelectronics, A*STAR (Agency for Science, Technology and Research), 11 Science Park Road, Singapore 117685, Singapore*

(Received 31 December 2012; accepted 11 March 2013; published online 21 March 2013)

Using stress-induced curved cantilevers to form double split-ring resonator (DSRR) in three-dimensional configuration, an electrically tunable microelectromechanical system (MEMS) based out-of-plane metamaterials THz filter is experimentally demonstrated and characterized. While the achieved tunable range for the resonant frequency is 0.5 THz at 20 V bias, quality factor of the resonant frequency is improved as well. This MEMS based THz filter using released DSRR structures shows its potential in tunable metamaterials applications such as sensors, optical switches, and filters. © *2013 American Institute of Physics*. [http://dx.doi.org/10.1063/1.4798244]

Recently, the electromagnetic (EM) metamaterials have received great attentions and obtained significant progress in development, since the metamaterials can exhibit permittivity and permeability with values which are not possible to get in nature.[1,2] Because of their unique and distinct reversed EM properties, diversified applications, such as high-resolution superlenses, invisibility cloaking devices, and perfect absorber, etc. have been investigated.[3–5] The realization of such extraordinary optical properties relies on the ability of metamaterials to create independently tailored electric and magnetic responses to incident radiation within or between the unit cells. However, metamaterials are limited to a fixed narrow spectral bandwidth. It will seriously affect and restrict their applications. Therefore, metamaterials filter whose operating frequency can be electrically adjusted is of great interest and importance to alleviate these limitations.

Currently, the tunability of metamaterials based on different structures to realize negative refractive index properties has been demonstrated by sophisticated fabrication technology and optimized designs.[6–12] With the aid of the tunability, reconfigurable metamaterial devices become feasible and show great potential in applications, e.g., sensors, switches, and filter, etc.[4,5] Within these devices, the tuning mechanisms include changing the surrounding media[6,7] and using semiconductors materials[11,12] to adjust the resonant frequency which are highly dependent on the nonlinear properties of the nature materials. However, these methods suffer from a limited tuning range as the small variation of material properties of surrounding media. On the other hand, microelectromechanical systems (MEMS) technology has been well developed for enabling complicated 3D micromechanical devices.[13,14] Tao *et al.* have reported a MEMS based metamaterials, which contains suspended and released silicon nitride ($SiN_x$) plates with a gold film pattern of single split-ring resonator (SRR) on each supported by two bimorph cantilevers plate to form a metamaterial unit cell. Due to the thermal expansion coefficient difference between the $SiN_x$ and gold films of the bimorph cantilever during the thermal cycle from 350 to 550 °C where such a metamaterials sample is heated up by using rapid thermal annealing (RTA) equipment, the two bimorph cantilevers bend upward and lifted up the released metamaterial unit cell plate. However, the achieved frequency tuning is less than 0.02 terahertz (THz) and the maximum change in transmission intensity is only 45%, while out-of-plane bending based actuation mechanism could not be controlled electrically at chip level, bulky RTA equipment is used.[8] Zhu *et al.* have demonstrated MEMS-based tunable metamaterials using in-plane movable metamaterial unit cells driven by electrostatic comb actuators.[9,10] While limited displacement, high driving voltages, and complicated bulk-silicon-micromachining process are drawbacks associated with these designs, the experimental results show that resonance condition is only two states at particular actuated position. In other words, no continuous change of resonant THz spectra has been achieved in this MEMS based metamaterial design.[10]

In this paper, we report a MEMS mechanism of active control metamaterials using electrostatic force to adjust the bending degree of surface micromachined double split-ring resonators (DSRR) structures. This tunable metamaterials THz filter having metallic DSRR released from silicon substrate is shown in Fig.1. The resonant frequency of the tunable metamaterials filter is a function of the refractive index of EM radiation, i.e., $n_{EM} = \sqrt{\mu(\omega) \cdot \varepsilon(\omega)}$, where the incident medium is lossless at normal incidence. The transmittance ($T$) can be expressed by[15]

$$T = \frac{4 n_{air} n_{sub} n_{EM}^2}{\left(n_{air} n_{sub} + n_{EM}^2\right)^2}, \tag{1}$$

where $n_{air}$ and $n_{sub}$ are the refractive index of air and silicon substrate respectively. According to the standard Drude-Lorentz model,[16] as shown in Eqs. (2) and (3), they stems from the universal resonant response of a harmonic oscillator to an external frequency-dependent perturbation

a)Author to whom correspondence should be addressed. Electronic mail: elelc@nus.edu.sg

 

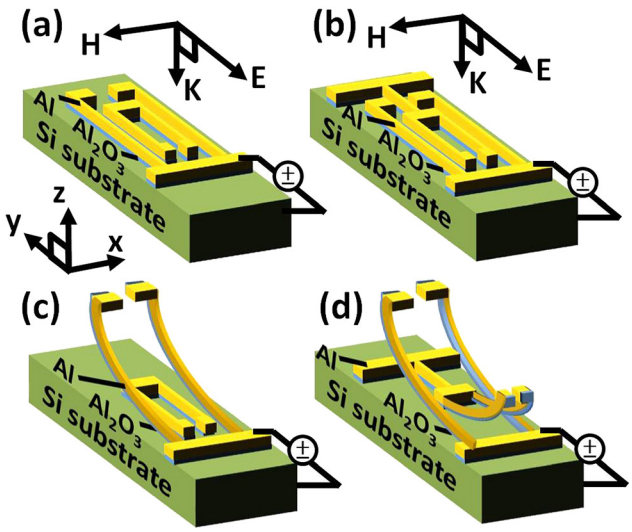


FIG. 1. Schematic diagrams of DSRR with (a) single-side, (b) double-side SICA; (c) and (d) show the snap-down DSRR structures because of electrostatic force which is a function of biased voltages on devices of (a) and (b), respectively.

$$\varepsilon(\omega) = 1 - \frac{F \cdot \omega_{pe}^2}{\omega^2 - \omega_{LCe}^2}, \tag{2}$$

$$\mu(\omega) = 1 - \frac{F \cdot \omega_{pm}^2}{\omega^2 - \omega_{LCm}^2}, \tag{3}$$

where $\omega_p$ is the plasma frequency, $\omega_{LC}$ is the resonant frequency, and $F$ is a dimensionless quantity, while subscripts $e$ and $m$ refer to electric and magnetic response. The resonant frequency can be obtained by $\omega_{LC} = 1/\sqrt{LC} = (c_0/l\sqrt{\varepsilon_C})\sqrt{d/w}$, where $c_0$ is the velocity of light in vacuum. Here, $C = \varepsilon_0\varepsilon_C wt/d$ and $L = \mu_0 l^2/t$ refer to the respective capacitance and inductance of gap within DSRR, where $w$ is the width of metal, $d$ is the width of capacitor gap, $t$ is the metal thickness, $l$ is the size of the DSRR, $\varepsilon_0$ is the free space permittivity, and $\varepsilon_C$ is the relative permittivity of the materials in the capacitor gap. The corresponding free-space wavelength, $\lambda_{LC} = l(2\pi)\sqrt{\varepsilon_C}\sqrt{w/d}$, is proportional to the size of DSRR. It indicates the proper design of features size for metamaterials structures can realize optical filters over frequencies that range from microwaves to UV.

Figures 1(a) and 1(b) show the schematic diagrams of DSRR in single-side and double-side released structure configuration. With properly controlled residual stress of released SRR, we can achieve optimized capacitance and inductance of gap within DSRR so as to determine $\omega_{LC}$. Besides, when we apply a DC bias between silicon substrate and these upward-bended cantilevers of SRR structures, these released and curved SRR cantilevers deflect toward silicon substrate due to the electrostatic force. Thus, we name these released SRR cantilevers as stress-induced curved actuators (SICAs). We can continuously change the bending degree of SICA in terms of DC bias value. As depicted in Figs. 1(c) and 1(d), the released SRR cantilevers will snap down to silicon substrate when the DC bias is higher than the pull-in voltage.[17] The feature sizes of metallic DSRR are chosen with split gap of 10 $\mu$m, the corresponding gap between the inner and outer ring is 6 $\mu$m, the width of the metal lines is 6 $\mu$m, and the length of the outer ring is 50 $\mu$m as shown in Fig. 2(a).

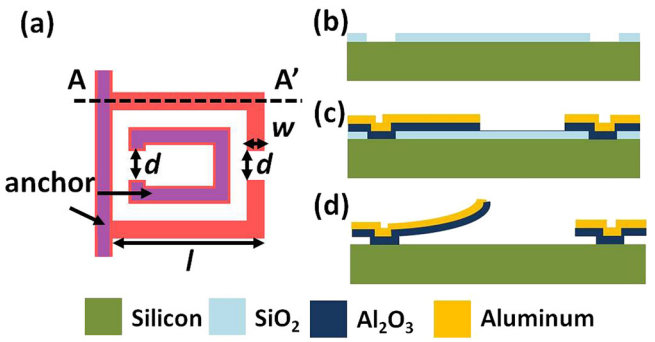


FIG. 2. (a) Unit cell layout of DSRR; ((b)–(e)) fabrication process along AA′ line in (a); (b) deposition and patterning of $SiO_2$ on Si substrate; (c) deposition and patterning of $Al_2O_3$ and Al layers; (e) released microstructures by using VHF.

To realize this device, a surface micromachining process is developed to demonstrate the metallic DSRR filter of large tuning range and low driving voltage. Figures 2(b)–2(d) show the fabrication process along AA′ line in Fig. 2(a). First, 100-nm-thick $SiO_2$ thin-film was deposited and patterned on a standard silicon wafer as shown in Fig. 2(b), and then deposited and patterned 20-nm-thick $Al_2O_3$ and 500-nm-thick Al, respectively, on surface (Fig. 2(c)). In order to create the upward-bended cantilevers of SRR structures to become out-of-plane SICAs, the vapor hydrogen fluoride (VHF) is applied to release the cantilevers (Fig. 2(d)).

As Figs. 3(a) and 3(b) show the SEM images of DSRR with single-side and double-side SICA, respectively, the curved SICA cantilevers can be obviously observed from different image contrast. The cantilever beam curves upward because the $Al_2O_3$ is under compressive residual stress while the Al film is under tensile residual stress. When a DC bias is applied between the SICA cantilevers and the substrate, electrostatic force pulls the SICA cantilevers from the original bending position (up state) to the snap-down position (down state) as shown in Figs. 3(c) and 3(d). In Fig. 4(a), the radius of curvature of SICA is expressed as a function of layer thickness by equation[18]

$$\frac{1}{\rho} = \frac{(\alpha_2 - \alpha_1)\cdot(T_2 - T_1)}{\frac{t_1 + t_2}{2} + \frac{2(E_1 I_1 + E_2 I_2)}{t_1 + t_2}\cdot\left(\frac{1}{E_1 t_1} + \frac{1}{E_2 t_2}\right)}, \tag{4}$$

where subscript 1 and 2 refer to $Al_2O_3$ and Al materials; $t$ is thickness of thin-films ($t_1 = 20$ nm and $t_2 = 500$ nm); $E$ is Young's modulus ($E_1 = 530$ GPa and $E_2 = 70$ GPa); $\alpha$ is coefficients of thermal expansion ($\alpha_1 = 8.1 \times 10^{-6}$ K$^{-1}$ and $\alpha_2 = 23.1 \times 10^{-6}$ K$^{-1}$); $I$ is area moment of inertia; $T$ is the temperature within fabrication process. When the devices were released, the radius of curvature is 32 $\mu$m calculated by Eq. (4). The radius of curvature is proportional to the thickness of Al layer. The measurement result of curvature is shown in Fig. 4(b). The cross-sectional image of outer ring for DSRR with single- and double-side SICA was observed by using optical microscope. The observed radius of curvature of SICA is 31.5 $\mu$m and bending height is 37 $\mu$m from doted white square in the zoom-in image as shown in

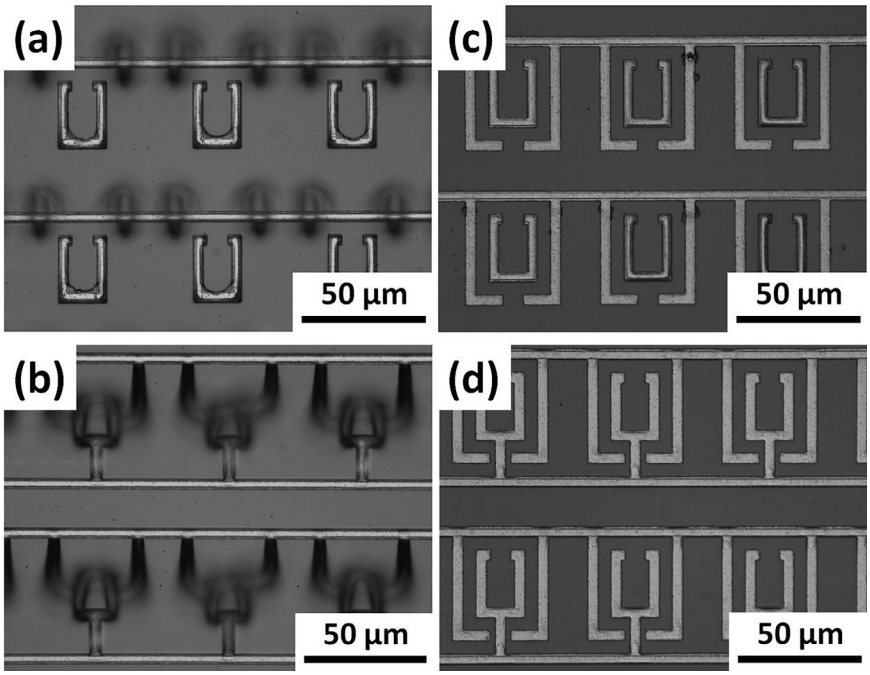


FIG. 3. SEM Images of DSRR with (a) single-side SICA and (b) double-side SICA after released microstructures; (c) and (d) are snap-down structures of (a) and (b), respectively.

Fig. 4(c). These observed values are comparable with modeling results in Fig. 4(a). It indicates that SICA cantilever having thicker Al layer and thinner $Al_2O_3$ layer can achieve larger radius of curvature. Referred to the capacitor equation $V \propto g/\rho$, the large radius of curvature and small gap between cantilever beams and substrate resulted in small driving voltage. However, the small gap will restrain the tunability of DSRR. It is a trade-off between driving voltage and tunable range of DSRR. Here, we chose the middle values of $Al_2O_3$ and Al layers thickness. The inset of Fig. 4(c) shows a drawing of SICA cantilever subjected to thermal and point-force loads. When a point force ($F$) is applied at tip of a released SICA cantilever, and the axial forces of $P_1$ and $P_2$ are generated with respect to the Al and $Al_2O_3$ layers. This SICA cantilever exhibits a very small gap at the joint of cantilever and substrate. The strong electrostatic force occurred at this small gap due to the applied DC bias will first pull down the portion of cantilever nearby the joint. Then, the adjacent gap become small as well and the portion of cantilever on top of this gap will be pulled down to substrate. Gradually, more portion of SICA cantilever is at down state. The final balanced position and shape of SICA cantilever is subject to the balance between electrostatic force and cantilever restoring force. By leveraging this unique curved cantilever structure, the driving voltage is reduced. This design significantly increase the moving range of the SRR structures compared with the counterparts using in-plane movable MEMS structures.[9,10]

The optical measurement results are black curves shown in Fig. 5. The transmission spectra of the DSRR with single-side and double-side SICA are measured without and with DC bias. Figure 5(a) shows the transmission spectrum of released DSRR with single-side SICA, and a peak is observed at 0.75 THz without biased voltage. By applying DC bias on SICA, the transmission peak is shifted from 0.75 THz to 0.25 THz as shown in Figs. 5(b) and 5(c) for 10 and 18 V bias, respectively. Further, Figs. 5(d)–5(f) show the peak of DSRR with double-side SICA can be tuned from 0.50 THz to 0.45 THz and 0.40 THz at 12 and 20 V bias, respectively. The tuning ranges of DSRR with single-side

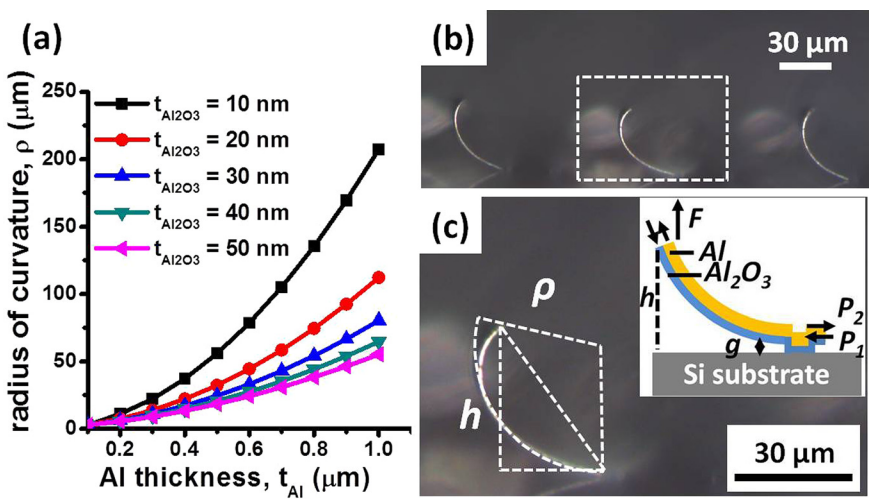


FIG. 4. (a) Radius of curvature of stress-induced curved beams as a function of layer thickness; (b) cross-sectional optical microscope image of DSRR with double-side SICA; (c) zoom-in image of doted white square in (b).

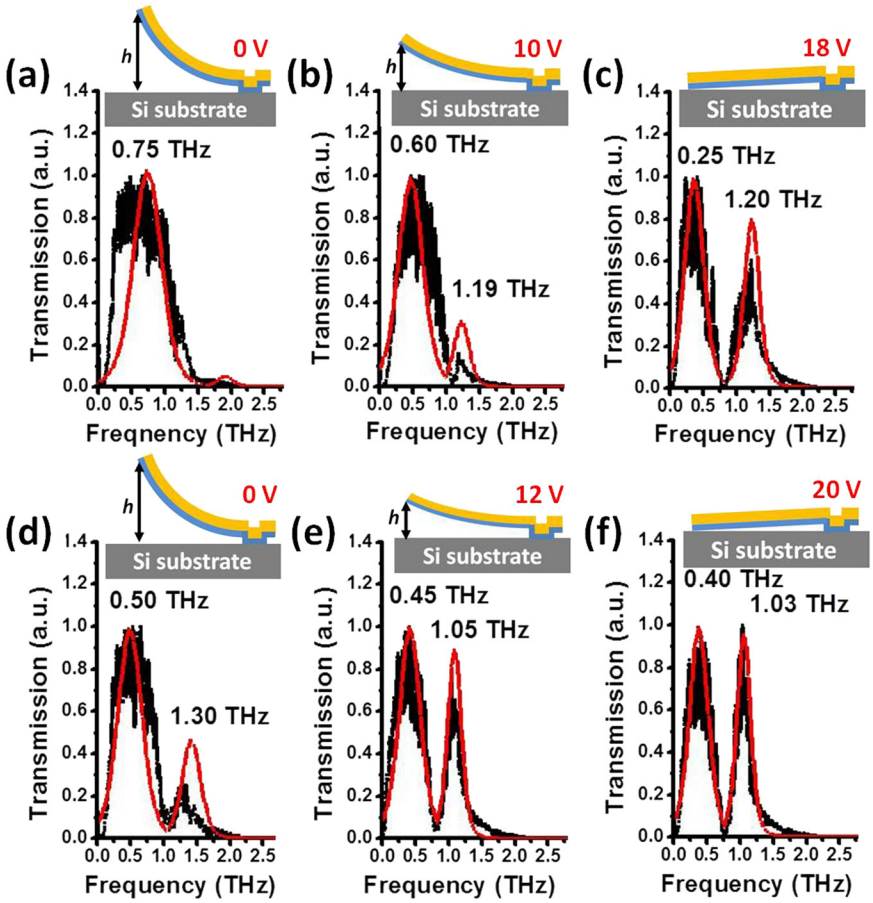


FIG. 5. The measured (black curve) and theoretical (red curve) transmission spectra of DSRR with ((a)–(c)) single-side, and ((d)–(f)) double-side SICA at different DC bias, respectively. Insets show the corresponding schematic bending height of ((a)–(f)).

and double-side SICA are observed as 0.5 THz and 0.1 THz at 20 V bias. The measurement results are comparable with theoretical spectra as shown in the red curves of Fig. 5.

Fig. 5 shows the transmission spectra with two resonant frequencies when the DSRR with single-side or double-side SICA are under bias. In such asymmetric SRR pairs, two splitting transmission can be interpreted by using the concept of plasmon hybridization model.[19] A sharp transmission peak within two hybridized modes is activated through the coupling among the asymmetric SRR elements. We experimentally validated this plasmon hybridization model proposed recently.[20,21] The intensity ratio of the first and second resonant frequency of THz filter with double-side SICA is increased for 3.7-fold, i.e., Fig. 5(f) versus Fig. 5(d). It is worth to mention that the Q-factor of second resonant frequency is also increased when the SICA is under bias. The second resonant frequency of DSRR with double-side SICA can be shifted from 1.30 to 1.03 THz, i.e., tuning range of 0.27 THz, and the Q-factor is enhanced for 1.27-fold at 20 V bias. This enhanced Q-factor shows that the DSRR THz filter has great potential in sensor applications. Moreover, it also exhibit wide tuning range under low driving voltage.

In conclusion, a tunable metamaterials using stress-induced cantilevers under electrostatic actuation scheme has been investigated as a DSRR THz filter of large frequency tuning range and high Q-factor. Experimental data show that the tuning range of resonant peak for DSRR with single-side SICA and double-side SICA are 0.50 THz and 0.27 THz, respectively. This tunable DSRR THz filter shows attractive features for potential applications in sensors and THz circuits.

This work was supported by Agency for Science, Technology and Research (A*STAR) under SERC Grant No. 1021650084.

[1]H. J. Lezec, J. A. Dionne, and H. A. Atwater, Science **316**, 430 (2007).
[2]J. Valentine, S. Zhang, T. Zentgraf, E. Ulin-Avila1, D. A. Genov1, G. Bartal1, and X. Zhang, Nature **455**, 376 (2008).
[3]J. B. Pendry, Phys. Rev. Lett. **85**, 3966 (2000).
[4]J. Hao, J. Wang, X. Liu, W. J. Padilla, L. Zhou, and M. Qiu, Appl. Phys. Lett. **96**, 251104 (2010).
[5]N. I. Zheludev, Science **328**, 582 (2010).
[6]H.-T. Chen, W. J. Padilla J. M. O. Zide, A. C. Gossard, A. J. Taylor, and R. D. Averitt, Nature **444**, 597 (2006).
[7]F. Zhang, L. Kang, Q. Zhao, J. Zhou, X. Zhao, and D. Lippens, Opt. Express **17**, 4360 (2009).
[8]H. Tao, A. C. Strikwerda, K. Fan, W. J. Padilla, X. Zhang, and R. D. Averitt, Phys. Rev. Lett. **103**, 147401 (2009).
[9]W. M. Zhu, A. Q. Liu, X. M. Zhang, D. P. Tsai, T. Bourouina, J. H. Teng, X. H. Zhang, H. C. Guo, H. Tanoto, T. Mei, G. Q. Lo, and D. L. Kwong, Adv. Mater. **23**, 1792 (2011).
[10]W. M. Zhu, A. Q. Liu, W. Zhang, J. F. Tao, T. Bourouina, J. H. Teng, X. H. Zhang, Q. Y. Wu, H. Tanoto, H. C. Guo, G. Q. Lo, and D. L. Kwong, Appl. Phys. Lett. **99**, 221102 (2011).
[11]K. A. Boulais, D. W. Rule, S. Simmons, F. Santiago, V. Gehman, K. Long, and A. Rayms-Keller, Appl. Phys. Lett. **93**, 043518 (2008).
[12]Z. L. Samson, K. F. MacDonald, F. De Angelis, B. Gholipour, K. Knight, C. C. Huang, E. Di Fabrizio, D. W. Hewak, and N. I. Zheludev, Appl. Phys. Lett. **96**, 143105 (2010).
[13]K. H. Koh, T. Kobayashi, J. Xie, A. Yu, and C. Lee, J. Micromech. Microeng. **21**, 075001 (2011).
[14]K. H. Koh and C. Lee, J. Microelectromech. Syst. **21**, 1124 (2012).
[15]M. E. Motamedi, W. H. Southwell, and W. J. Gunning, Appl. Opt. **31**, 4371 (1992).
[16]C. M. Soukoulis, M. Kafesaki, and E. N. Economou, Adv. Mat. **18**, 1941 (2006).
[17]Y.-J. Lai, C. Lee, C.-Y. Wu, W.-C. Chen, C. Chen, Y.-S. Lin, W. Fang, and R.-S. Huang, Jpn. J. Appl. Phys. **42**, 4067 (2003).

[18]M. Shavezipur, W. Guo, C. Carraro, and R. Maboudian, J. Microelectromech. Syst. **21**, 541 (2012).
[19]H. C. Guo, N. Liu, L. W. Fu, T. P. Meyrath, T. Zentgraf, H. Schweizer, and H. Giessen, Opt. Express **15**, 12095 (2007).
[20]S. Zhang, D. A. Genov, Y. Wang, M. Liu, and X. Zhang, Phys. Rev. Lett. **101**, 047401 (2008).
[21]P. Tassin, L. Zhang, T. Koschny, E. N. Economou, and C. M. Soukoulis, Phys. Rev. Lett. **102**, 053901 (2009).